Pharmaceutical Modeling

Discovery of Potent, Reversible and Competitive Cruzain Inhibitors with Trypanocidal Activity: A Structure-Based Drug Design Approach

Mariana L Souza, Celso de Oliveira Rezende Júnior, Rafaela Salgado Ferreira, Rocio M Espinoza Chávez, Leonardo Luiz Gomes Ferreira, Brian W Slafer, Luma Godoy Magalhaes, Renata Krogh, Glaucius Oliva, Fabio C Cruz, Luiz Dias, and Adriano Defini Andricopulo

Just Accepted

Title

Discovery of Potent, Reversible and Competitive Cruzain Inhibitors with Trypanocidal Activity: A Structure-Based Drug Design Approach

Authors

Mariana L. de Souza[1]*, Celso de Oliveira Rezende Junior[2]*, Rafaela S. Ferreira[3], Rocio Marisol Espinoza Chávez[2], Leonardo L. G. Ferreira[1], Brian W. Slafer[2], Luma G. Magalhães[1], Renata Krogh[1], Glaucius Oliva[1], Fabio Cardoso Cruz[4], Luiz Carlos Dias[2]**, Adriano D. Andricopulo[1]**

Affiliations

[1]Laboratory of Medicinal and Computational Chemistry, Physics Institute of Sao Carlos, University of Sao Paulo, Sao Carlos – SP, 13563-120, Brazil

[2]Institute of Chemistry, State University of Campinas, Campinas – SP, 13084-971, Brazil

[3]Department of Biochemistry and Immunology, Federal University of Minas Gerais, Belo Horizonte – MG, 31270-901, Brazil

[4]Department of Pharmacology, Federal University of Sao Paulo, Sao Paulo – SP, 04023-062, Brazil

*These authors contributed equally to this work

**Correspondence: aandrico@ifsc.usp.br (A.D.A); ldias@iqm.unicamp.br (L.C.D)

1
2
3
4
5
6
7
8
9
10
11
12
13
14
15
16
17
18
19
20
21
22
23
24
25
26
27
28
29
30
31
32
33
34
35
36
37
38
39
40
41
42
43
44
45
46
47
48
49
50
51
52
53
54
55
56
57
58
59
60

2

ABSTRACT

A virtual screening conducted with nearly 4,000,000 compounds from lead-like and fragment-like subsets enabled the identification of a small-molecule inhibitor (**1**) of the *Trypanosoma cruzi* cruzain enzyme, a validated drug target for Chagas disease. Subsequent comprehensive structure-based drug design and structure-activity relationship studies led to the discovery of carbamoyl imidazoles as potent, reversible and competitive cruzain inhibitors. The most potent carbamoyl imidazole inhibitor (**45**) exhibited high affinity with a K_i value of 20 nM, presenting both *in vitro* and *in vivo* activity against *T. cruzi*. Furthermore, the most promising compounds reduced parasite burden *in vivo* and showed no toxicity at a dose of 100 mg/kg. These carbamoyl imidazoles are structurally attractive, nonpeptidic, and easy to prepare and synthetically modify. Finally, these results further advance our understanding of the noncovalent mode of inhibition of this pharmaceutically relevant enzyme, building strong foundations for drug discovery efforts.

Keywords: Chagas disease, virtual screening, organic synthesis, structure-activity relationships, drug design, drug discovery, SBDD, neglected tropical diseases

INTRODUCTION

Chagas disease is a major cause of death and heart failure in Latin America.[1] This neglected tropical disease (NTD) has also become a relevant public health problem in nonendemic countries in North America and Europe and in the Western Pacific region.[2] According to the World Health Organization (WHO), approximately 8 million people worldwide are infected with the protozoan *Trypanosoma cruzi*, the etiological agent of Chagas disease. In addition, Chagas disease causes 10,000 deaths annually, and more than 25 million people are at risk of infection.[3]

Chemotherapy for Chagas disease is obsolete; no therapeutic novelty has entered clinical practice since the early 1970s. This is one of the most remarkable examples of a lack of pharmaceutical innovation in an area. The only two available drugs, nifurtimox and benznidazole, are nitroheterocyclic compounds that cause severe adverse effects in up to 40% of patients and are effective only in the acute phase of the disease.[2] For instance, nifurtimox was discontinued in Brazil, Argentina, Chile and Uruguay because of its remarkable toxicity, which frequently causes adverse effects such as anorexia, weight loss, psychiatric problems, insomnia, nausea, intestinal colic and diarrhea.[4] Consequently, patients in the chronic stage of the disease, which include those with chagasic cardiomyopathy, are completely deprived of adequate treatments. Considering these shortcomings, developing safe and effective drugs for Chagas disease has been headlined as an urgent need by the global scientific community and international health agencies.[5]

The enzyme cruzain (EC 3.4.22.51), the major cysteine protease from *T. cruzi*, is expressed during the entire life cycle of the parasite and is essential to several physiological processes, including nutrition, circumvention of the host immune response, and invasion of host cells.[6,7] Validation of cruzain as a pharmacological target has relied on multiple studies on the molecular biology of *T. cruzi* along with proof-of-concept investigations showing that initial cruzain inhibitors reduce parasite load in murine models of Chagas disease.[8,9] Following these findings, different inhibitor classes have been discovered, comprising peptidic and nonpeptidic, and covalent and noncovalent inhibitors. Some examples include vinyl sulfones, fluoromethyl ketones, triazoles, pyrimidines, thiosemicarbazones, chalcones and benzimidazoles.[6,9-16] The vinyl sulfone K777, which binds irreversibly to the catalytic thiol group of Cys25 through a Michael addition, is a high-affinity cruzain inhibitor with remarkable *in vivo* trypanocidal activity.[17,18] Although K777 yielded inspiring results in preclinical tests, toxicity-related issues were raised and were associated with the covalent mode of action of the inhibitor, preventing the candidate from progressing into advanced clinical development.[9] The results of these investigations along with the available X-ray structures of the enzyme bound to small-molecule inhibitors have been fundamental to foster existing studies aimed toward the discovery of novel inhibitor classes with a different mode of enzyme inhibition.

Structure-based drug design (SBDD) approaches have significantly contributed to the generation of new hits covering diverse chemical spaces and to the optimization of lead compounds for a variety of biologically relevant enzymes. In particular, reversible inhibition is an effective means of modulating the enzymatic activity of

5

relevant drug targets. For instance, competitive inhibitors specifically target the free enzyme (E) to form a binary enzyme-inhibitor (E–I) complex, competing with the substrate for binding. This phenomenon provides unique opportunities for enzyme inhibitor drug discovery and the optimization of multiple important properties, such as potency, affinity and selectivity.

Considering the current context of Chagas disease drug discovery, the main goal of this work was the design and optimization of novel, reversible and competitive cruzain inhibitors with *in vitro* and *in vivo* anti-*T. cruzi* activity. This goal was pursued by conducting a computational-experimental integrated approach involving SBDD, organic synthesis, biochemical and biological *in vitro* assays and *in vivo* evaluation. To achieve this general purpose, we settled the following specific goals: (i) the development of a virtual screening workflow aimed at the selection of virtual hits for further *in vitro* profiling; (ii) the use of molecular docking to the design of analogs of virtual hits that proved to be active; (iii) the synthesis of the designed compounds; (iv) the *in vitro* evaluation of the synthesized analogs against cruzain; (v) the determination of the mechanism of action of the most potent compounds; (vi) the evaluation of the *in vitro* trypanocidal activity and cytotoxicity of the most potent cruzain inhibitors; (vii) and finally the evaluation of the *in vivo* acute toxicity and efficacy of the most promising compounds. This work has a distinctive character among the current literature[6,9-16] since it describes the discovery of reversible and competitive cruzain inhibitors with *in vivo* efficacy from a virtual screening effort using a comprehensive combination of computational, synthetic and biological approaches.

MATERIALS AND METHODS

Virtual Screening and Molecular Docking

The lead-like and fragment-like subsets containing 3,409,091 and 453,539 molecules, respectively, were prepared from SMILES files downloaded from ZINC (University of California at San Francisco – UCSF).[19] The X-ray cruzain structure (PDB 3KKU, 1.28 Å)[20] was prepared by removing water molecules and ligands and adding hydrogen atoms. Enrichment plots were generated using DOCK 3.5.54 and a set of 146 competitive cruzain inhibitors that were previously described.[20] The best curve, in which His162 and Cy25 were kept protonated and negatively charged, respectively, yielded an enrichment factor of 40 at 1% of the database, corresponding to an AUC of 0.9313 (see Figure S1 in the Supporting Information). In the SBVS using DOCK 3.5.54[21] (UCSF), the molecular surface was generated, and energy potential grids calculated using CHEMGRID[22] and Delphi.[23] Multiple pre-calculated conformations of ligands were docked, and each pose was scored based on van der Waals and electrostatic interactions and ligand desolvation. In the SBVS using GOLD 4.2[24] (Cambridge Crystallographic Data Centre – CCDC, Cambridge, UK) compounds were docked applying the default parameters and GoldScore function. The binding site was defined as a sphere with a 10 Å radius centered on the coordinates of the Cys25 sulfur atom. In the SBVS using the Surflex[25] module of Sybyl 8.0 (Certara, Princeton, NJ), the protomol was generated based on the crystallographic ligand. The Surflex default scoring function was used to score the docking solutions.[26]

7

Examination of the docking output from all used programs was carried out with Pymol[27] (Schrödinger, New York, NY) and Chimera[28] (UCSF) (see Figure S2 in the Supporting Information for the detailed workflow of the SBVS). Virtual screening hits were purchased from ENAMINE (Kiev, Ukraine).

Cruzain Expression, Activation and Purification

Cruzain was expressed and purified using a modified version of a previously published protocol.[12] *Escherichia Coli* (SG13009 strain) harboring the pETM11 plasmid which contains the codifying sequence for cruzain was pre-inoculated in 150 mL of Luria Bertani (LB) medium supplemented with gentamicin (20 μg/mL) and kanamicin (50 μg/mL). The cultures were kept overnight at 37 °C under agitation (200 rpm). Next, the cultures were added to a medium (1 L) consisting of triptone (10%), yeast extract (5%), 25 mM $NaHPO_4$, 25 mM KH_2PO_4, 50 mM NH_2Cl, 5 mM Na_2SO_4, glycerol (0.5%), glucose (0.5%), lactose (0.2%), and 2 mM $MgSO_4$. The cultures were kept at 37 °C under agitation (200 rpm) until reaching an optical density (OD_{600}) of 0.16, which was followed by incubation for 72 hours at 18 °C. Next, the cells were harvested by centrifugation at 5000 rpm (30 minutes, 4 °C) and the pellet suspended in 200 mL of lysis buffer (300 mM NaCl, 50 mM Tris, 10 mM imidazole, 1 mM $CaCl_2$, 1 mM $MgSO_4$, pH 10). This was followed by sonication (12 cycles of 30 seconds) and centrifugation at 9000 rpm (30 minutes, 4 °C). The supernatant was incubated for 3 hours at 4 °C with Ni-NTA Superflow resin (5 mL) (Qiagen, Hilden, Germany) for subsequent Immobilized Metal Affinity Chromatography purification

8

(IMAC). The resin was washed with buffer (300 mM NaCl, 50 mM Tris, 10 mM imidazole, pH 10). Next, the resin was washed with increasing concentrations of imidazole (25, 50, 75, 100 and 250 mM). The fractions containing the protein (75 − 250 mM imidazole) were dialyzed in acetate buffer 0.1 M pH 5.5 and concentrated to 0.5 mg/mL in activation buffer (100 mM NaAc, 300 mM NaCl, 5 mM EDTA, 10 mM DTT, pH 5.5). The N-terminal of cruzain was cleaved by autoproteolysis in the activation buffer to produce the active enzyme. This process was monitored by the cleavage of the substrate Z-Phe-Arg-AMC and confirmed by SDS PAGE (12%) gel electrophoresis. Next, active cruzain was dialyzed in buffer (20 mM NaAc, 150 mM NaCl, pH 7.2) and mixed with Thiopropyl Sepharose 6B resin (GE Healthcare Life Sciences, Pittsburgh, PA) previously equilibrated with the same buffer, and stored overnight at 4 ^{o}C under gentle agitation. The elution of the active protein was carried out by washing the resin with 20 mM DTT buffer. The protein solution was filtrated using Amicon filter (Sigma-Aldrich, St. Louis, MO) and stored at − 80 ^{o}C in buffer (0.1 M NaAc, 0.000005% Triton X-100, pH 5.5).

Enzyme Kinetics

Cruzain activity was measured by monitoring the cleavage of the fluorogenic substrate Z-Phe-Arg-AMC as previously described.[12] Assays were performed in 0.1 M sodium acetate, 5 mM DTT and 0.01% Triton X-100, pH 5.5. Cruzain concentration was 1 nM and substrate concentration was 5.0 μM (K_m = 1.6 μM). For K_i determination, several substrate concentrations were used. Assays were followed for

9

300 seconds at 30 °C in 96-well flat bottom black plates, and activity was calculated based on initial rates compared to a DMSO control. A known reversible and competitive cruzain inhibitor was used as a positive control in all enzyme assays.[12] Wavelengths of 355 nm and 460 nm were used for excitation and emission, respectively. The IC_{50} values were determined by using at least six inhibitor concentrations, each one evaluated in triplicate. To determine the mechanism of inhibition, eight substrate concentrations (0.31 to 40 µM) were used in 2-fold increments. K_i values were determined from Lineweaver-Burk plots generated in SigmaPlot 10.0 (Systat Software Inc., Erkrath, Germany). The assays for the identification of the mechanism of inhibition were performed in triplicates in two independent experiments. SigmaPlot was used to determine the IC_{50} and K_i values.

Trypanosoma cruzi Culture Procedures

In vitro assays were performed using *T. cruzi* Tulahuen strain, provided by Frederick S. Buckner (University of Washington, Seattle, WA), genetically engineered to express the *E. coli* β-galactosidase gene (*lacZ*).[29] Epimastigotes were grown in liver infusion tryptone (LIT) medium supplemented with 10% fetal calf serum (FCS), penicillin and streptomycin. Metacyclogenesis to trypomastigotes was induced by seeding epimastigotes in Grace's Insect Medium (Sigma-Aldrich, St. Louis, MO) supplemented with 10% FCS. After differentiation, metacyclic trypomastigotes were harvested and transferred to test plates.

Intracellular *Trypanosoma cruzi* Amastigote Assays

Intracellular amastigote assays were performed in 96-well tissue culture plates. HFF-1 human fibroblasts were seeded at 2×10^3 cells per well in DMEM medium (80 μL) without phenol red and incubated overnight at 37 °C in a 5% CO_2 humidified atmosphere. In the next day, trypomastigotes were added at 1×10^4 cells per well. After 24 hours, medium was removed to clear extracellular parasites, and 100 μL of fresh DMEM medium were added to each well. Next, 50 μL of cruzain inhibitors were added in serial dilutions to yield final concentrations of 0.1 – 100 μM. The compounds were tested at seven concentrations in 3-fold dilutions, each concentration being tested in duplicate in three independent experiments. The plates were incubated for 120 hours at 37 °C in a 5% CO_2 humidified atmosphere. All plates included multiple wells with infected fibroblasts without the addition of any inhibitor (negative controls) and wells with **BZ** (Sigma-Aldrich, St. Louis, MO) as positive controls. After incubation, 50 μL of 1mM chlorophenol red β-D-galactopyranoside (CPRG, Sigma-Aldrich, St. Louis, MO) and 0.1% Igepal CA-630 (Sigma-Aldrich, St. Louis, MO) were added to each well and absorbance was measured at 570 nm. Data were transferred to SigmaPlot to determine the IC_{50} values.

Cytotoxicity

Cytotoxicity was evaluated using HFF-1 human fibroblasts and the MTS Tetrazolium assay[30] (Promega, Madison, WI). Fibroblasts were seeded at 2×10^3 cells

per well in DMEM medium (80 μL) supplemented with 10% FCS in 96-well plates and incubated overnight at 37 °C in a 5% CO_2 humidified atmosphere. In the next day, 20 μL of cruzain inhibitors were added in serial dilutions to yield final concentrations of 0.1 –100 μM, and the plates were incubated for 72 hours. Compounds were tested at seven concentrations in 2-fold dilutions, each dilution being tested in triplicate in two independent experiments. After 72 hours, 20 μL of MTS were added to the wells. After 4 hours of incubation, absorbance was measured at 490 nm to assess MTS reduction by viable cells. All plates included multiple wells with viable fibroblasts without the addition of any inhibitor (negative controls). Doxorubicin (Sigma-Aldrich, St. Louis, MO) was used as positive control. Data were transferred to SigmaPlot to determine the IC_{50} values.

In vivo Assays

Pathogen-free female Swiss mice weighing 25 – 30 g, obtained from the animal breeding facility of the University of Sao Paulo, were used in the *in vivo* toxicity and efficacy studies. Groups of five mice were housed in Ventilife mini-isolators (Alesco, Sao Paulo, Brazil) in rooms maintained at 23 ± 2 ºC. The animals were continuously maintained on a light cycle (12/12 hours, lights off at 08:00 p.m.) with unrestricted access to food and water. The experimental protocol was approved by the Ethics Committee on the Use of Animals of the Sao Paulo Federal University (Protocol number 5301080816) and was conducted according to the ethics principles of the National Council for Animal Experimentation Control (CONCEA, Brazil).

12

The following solutions were prepared for the *in vivo* assays: (i) vehicle: 0.9% NaCl, 10% DMSO in distilled water; (ii) reference drug: **BZ** (Sigma-Aldrich, St. Louis, MO), 0.9% NaCl, 10% DMSO in distilled water; (iii) compounds: cruzain inhibitors **1** and **45**, 0.9% NaCl, 10% DMSO in distilled water.

In vivo toxicity (MTD) was determined by testing increasing doses of compounds on distinct groups of mice (2 animals per group).[31] Non-infected Swiss female mice were divided into 6 groups and treated via i.p. with four different doses of each compound (75, 100, 150, and 300 mg/kg). Each mouse received a single dose of the testing compounds. The animals were observed for seven days according to the OECD guidelines, which include the following: (i) behavioral functions – alertness, restlessness, irritability, and fearfulness; (ii) neurological activity – spontaneous activity, reactivity, touch response, pain response, and gait; and (iii) autonomic functions – defecation and urination. Animals that received vehicle solution (0.9% NaCl, 10% DMSO solution) were used as the control group.

Bloodstream *T. cruzi* trypomastigotes (*Y* strain) collected from infected Swiss mice were used to infect the animals used in the *in vivo* studies. This strain, originally isolated from an acute-phase chagasic patient in 1950 in Sao Paulo, Brazil, is known for producing high levels of parasitemia and killing 100% of the animals between days 12 and 20 after infection.[32]

Four-week-old female Swiss mice (5 animals per group) were inoculated (i.p.) with 5×10^5 trypomastigotes. Parasitemia was monitored daily by counting the number of motile parasites in 5 µL of blood drawn from the lateral tail vein as described by Brener.[33] At the fifth day after infection, mice showing positive

parasitemia were randomly selected and treated (i.p.) with seven daily doses of **BZ** and compounds **1** and **45** (100 mg/kg of body weight), and vehicle. The mortality rate was expressed as the cumulative percentage of deaths during a period 15 days after infection.

Data were submitted to Repeated Measures ANOVA (Statistics Solutions, Clearwater, FL). The ANOVA bifactorial module was used to correlate parasitemia and treatment duration (parasitemia curve). The ANOVA monofactorial module was used to analyze peak parasitemia. When the ANOVA statistics yielded significant results (p-value < 0.05), F-test analyses were performed to determine the statistical significance of intergroup comparisons. The survival rate curves were submitted to Chi-square analyses.

RESULTS AND DISCUSSION

The present work employed an SBDD approach to identify a new chemically diverse group of competitive cruzain inhibitors, combining experimental and computational methods. Structure-based virtual screening (SBVS) studies were performed with three different molecular docking algorithms and the top-scoring compounds making the most relevant molecular intermolecular interactions, according to the available cruzain-inhibitor X-ray structures, were selected (see Figure S2 in the Supporting Information for the detailed SBVS workflow). Compounds containing aromatic, hydrophobic or positively charged groups interacting with the S2 pocket in the enzyme active site were prioritized. Additionally, previously described cruzain

14

inhibitors have been shown to form hydrogen bonds with Gln19, Asp161 and Gly66, which are located at the S1, S1' and S3 subsites, respectively. Compounds interacting with these residues were also privileged when selecting candidates for experimental evaluation. Based on this rationale, the complete SBVS process led to the selection of 14 lead-like and four fragment-like compounds (Figure 1A) for experimental investigation.
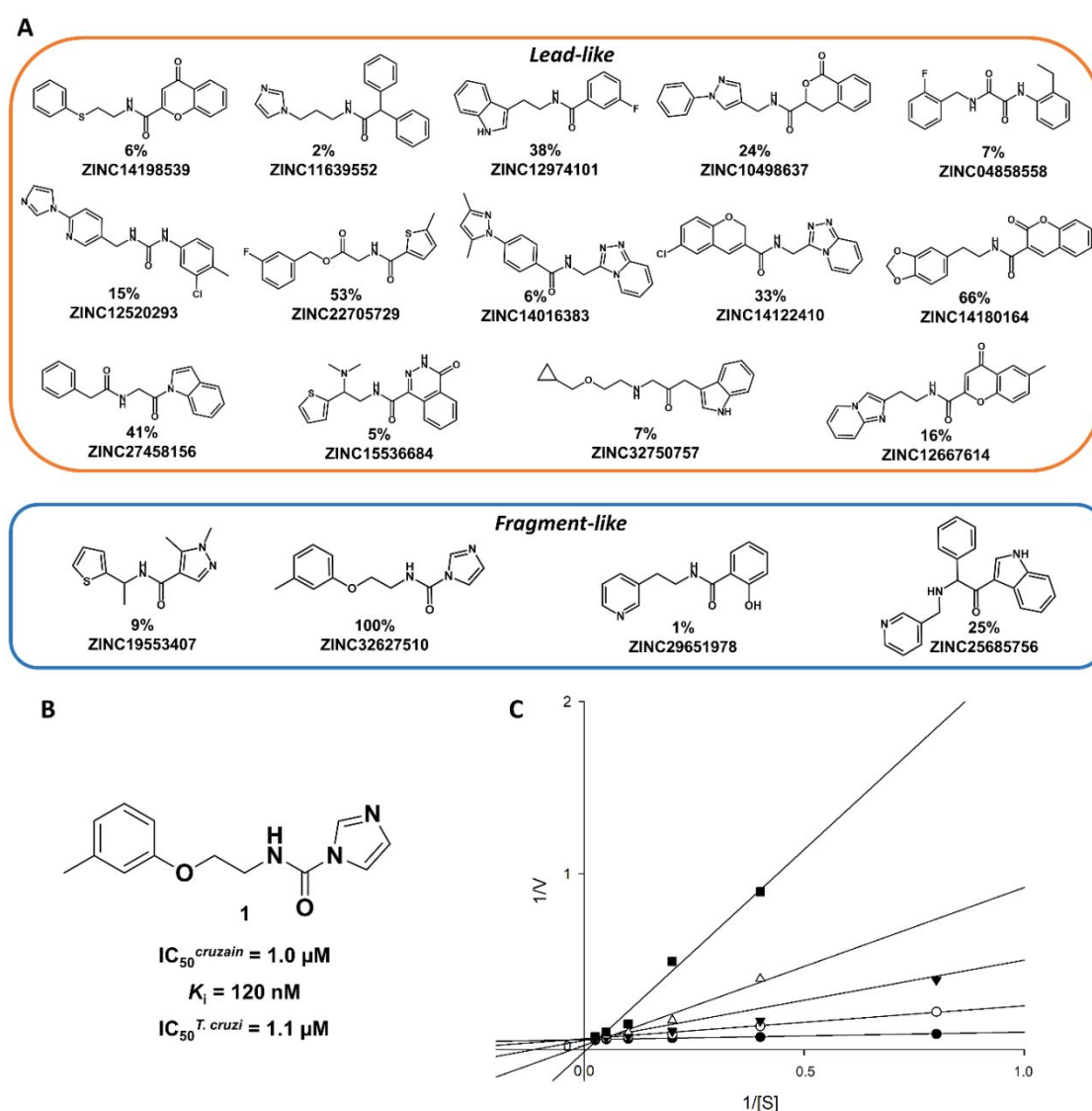

Figure 1. Structure-based virtual screening (SBVS) hits. (A) Structures of the SBVS hits and the corresponding percent inhibition at 100 μM against the cruzain enzyme. (B) Structure of compound **1**, which was identified in a SBVS as a novel, noncovalent and nonpeptidic cruzain inhibitor. (C) Lineaweaver-Burk plot showing the

15

competitive mechanism of inhibition of compound **1**. Curves refer to the following inhibitor concentrations: control – no inhibitor (●); 0.3 μM (○); 0.6 μM (▼); 1.25 μM (△) and 2.50 μM (■).

The eighteen SBVS hits were evaluated in enzyme kinetics assays for their activity against cruzain. A fluorescence test relying on the cleavage rate of the fluorogenic substrate Z-Phe-Arg-AMC was used.[34] The most potent inhibitor from the fragment-like library was compound **1** (ZINC3267510, Figure 1B), which had an IC_{50} value of 1 μM. Compound **1** proved to be a competitive and reversible inhibitor of cruzain (K_i = 120 nM), as demonstrated in the Lineaweaver-Burk plot depicted in Figure 1C. The activity of compound **1** on cruzain was neither time dependent nor detergent sensitive.[35] Given these results, inhibitor **1** was tested for its *in vitro* activity against *T. cruzi* (Tulahuen *LacZ*), yielding an IC_{50} of 1.1 μM, which is 3-fold better than that of the standard drug benznidazole (**BZ**, IC_{50} = 3.3 μM, Table 5). In addition, compound **1** features a ligand efficiency (LE)[36,37] of 0.53 kcal·mol^{-1}/non-H atom, which is a suitable value for fragment-based ligand optimization.

Considering the gathered data, cruzain inhibitor **1** was used as the lead for molecular optimization and structure–activity relationship (SAR) studies. A series of analogs were designed considering the predicted binding mode and intermolecular interactions between **1** and the binding site of cruzain (Figure 2A). The phenyl ring of compound **1** was observed to interact with the S2 subsite, which is known for accommodating hydrophobic groups. The urea nitrogen acted as a hydrogen bond donor to the carbonyl of Asp161, and the urea oxygen formed a hydrogen bond with the sidechain of Gln19. Another hydrogen bond occurred between the imidazole in **1**

and the indole nitrogen of Trp184. A π stacking interaction was observed between imidazole rings of the inhibitor and His162. These observations led to the splitting of **1** into three fragments as the spots for structural modification, namely, the phenyl, the linker between the rings, and the imidazole (Figure 2B). In the next subsection, we describe the organic synthesis efforts, which involved the synthesis of virtual screening hit **1** and its analogs.
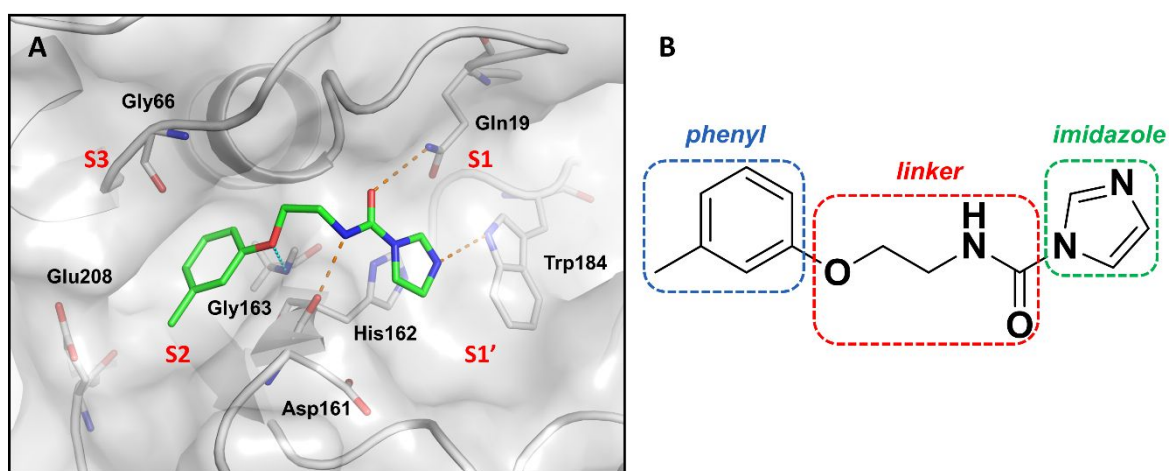

Figure 2. Cruzain inhibitor 1 identified in the structure-based virtual screening (SBVS). (A) Predicted binding mode of inhibitor **1** in the active site of cruzain (PDB 3KKU, 1.28 Å). Cruzain is depicted in cartoon and surface representations. Cruzain amino acid residues (carbon in white) and **1** (carbon in green) are illustrated as sticks. Subsites in the cruzain binding site are labeled S1, S1', S2 and S3. Intermolecular interactions are indicated as dashed lines. (B) Structure of **1** highlighting the splitting of the compound into three fragments as a strategy for molecular optimization.

Organic Synthesis

Synthesis of the virtual screening hit **1** and the analogs having different substituents at the phenyl ring are shown in Scheme 1. Hydrochloride salts **15-27** and

17

43-44 were prepared from the corresponding substituted phenols **2-14** and **40-41**, respectively, by an S_N2 reaction using alkyl tosylate **42**, followed by Boc deprotection under acidic conditions. Subsequent reaction of these salts with carbonyldiimidazole (CDI) led to the formation of the target substituted imidazoles **1**, **28-39**, and **45-46**. Pyridyl analog **50** was prepared by an S_NAr reaction between dibromopyridine **47** and alcohol **48**, followed by Boc deprotection and acylation using CDI (Scheme 1).

Scheme 1. Synthesis of substituted imidazoles 1, 28-39, 45-46 and 50[a]
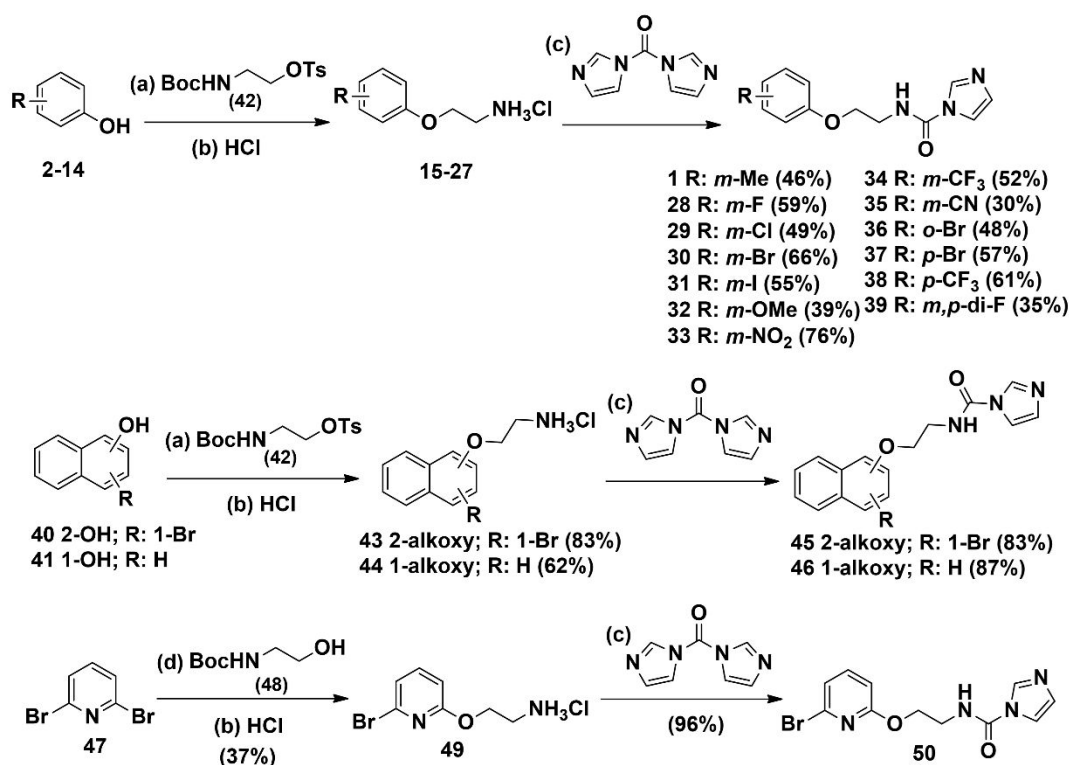
^{a}Reagents and conditions: (a) **42**, K_2CO_3, DMF, 60 °C, 6-10 h; (b) HCl (4 M in dioxane), DCM, rt, 2-7 h; (c) CDI, DMF, rt, 3-8 h; (d) I) **48**, NaH, THF, 0 °C to rt, 20 min; II) **47**, rt, 29 h.

Modifications on the linker between the aromatic rings of compound **1** were also explored. Replacement of the oxygen by nitrogen (NH) was not possible because the NH group attacks the activated carbonyl, leading to cyclic urea **53** instead of the desired product **52** (Scheme 2). To block this undesired cyclization reaction, an *N*-methyl (NMe) group, instead of an NH, was used to replace the oxygen in the linker fragment, leading to the formation of **56** (Scheme 3).

Scheme 2. Synthesis of compound 53[a]
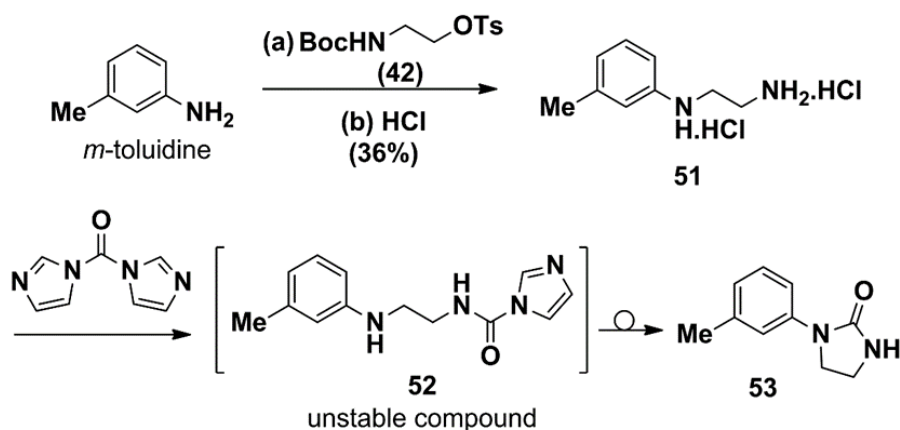
[a]Reagents and conditions: (a) 42, K_2CO_3, DMF, 18 h; (b) HCl (4M in dioxane), DCM, rt, 1 h; (c) CDI, DMF, rt, 3 h.

Scheme 3. Synthesis of amine 56[a]
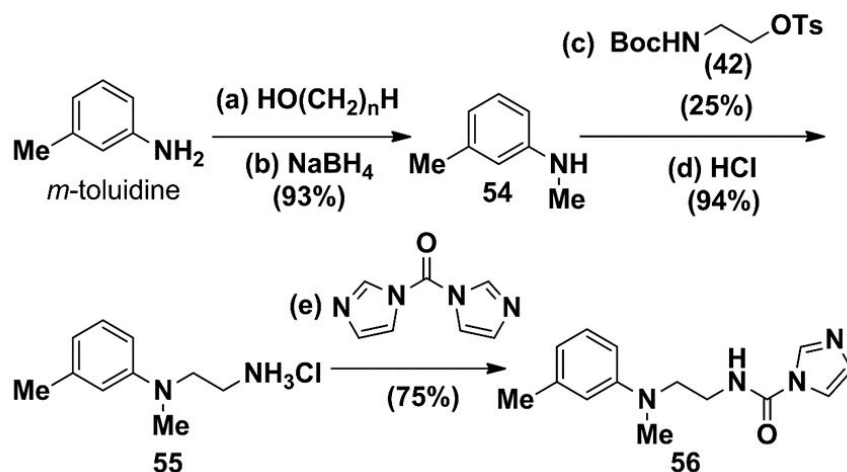
[a]Reagents and conditions: (a) *p*-formaldehyde, MeONa, MeOH, 65 °C, 1 h; (b) NaBH$_4$, 65 °C, 1.5 h; (c) I) NaH, THF, 0 °C to rt, 0.5 h; II) 42, 0 °C to rt, 5 h; (d) HCl (4M in dioxane), DCM, rt, 3 h; (e) CDI, DMF, rt, 3 h.

Methylaniline **54** was prepared from *m*-toluidine by reductive amination. This reaction intermediate was then alkylated using tosylate **42**, followed by Boc deprotection and acylation with CDI to afford **56** (Scheme 3). Ester and amide derivatives **60** and **61** were prepared from the corresponding phenol and aniline by esterification and amidation, respectively, using carboxylic acid **57**, followed by Boc deprotection and acylation with CDI (Scheme 4).

Scheme 4. Synthesis of esters 60 and 63 and amide 61[a]
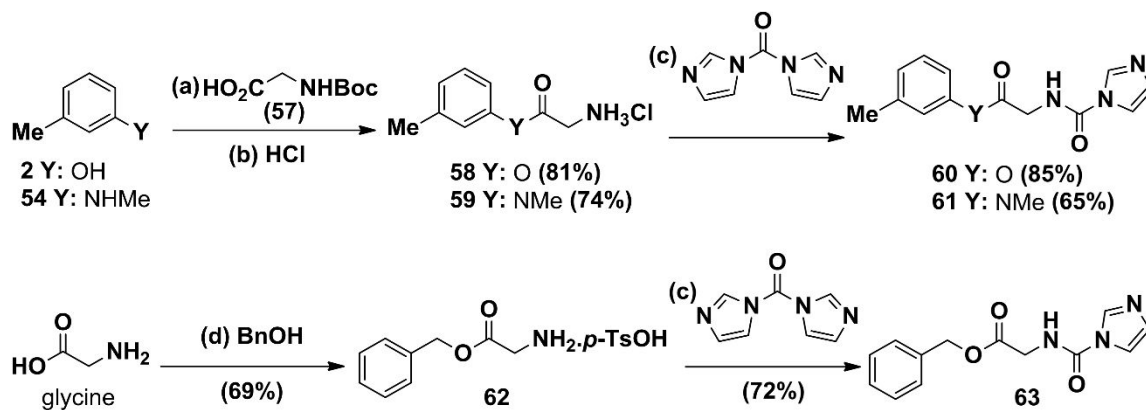
[a]Reagents and conditions: (a) **57**, EDC, DMAP for **60**, and HOBt for **61**, DCM, rt, 2-4 h; (b) HCl (4M in dioxane), DCM, rt, 3 h; (c) CDI, DMF, rt, 3 h; (d) BnOH, *p*-TsOH, toluene, 100 °C, 18 h.

Benzylic ester **63** was prepared from glycine by esterification using benzyl alcohol and *p*-TsOH, followed by acylation with CDI (Scheme 4). Esters **68-71** were

20

prepared from the carboxylic acids of benzene, pyrazole, furan, and naphthalene, respectively (Scheme 5). The corresponding carboxylic acids were treated with alcohol **48**, followed by Boc deprotection and acylation using CDI.

Scheme 5. Synthesis of esters 68-71[a]
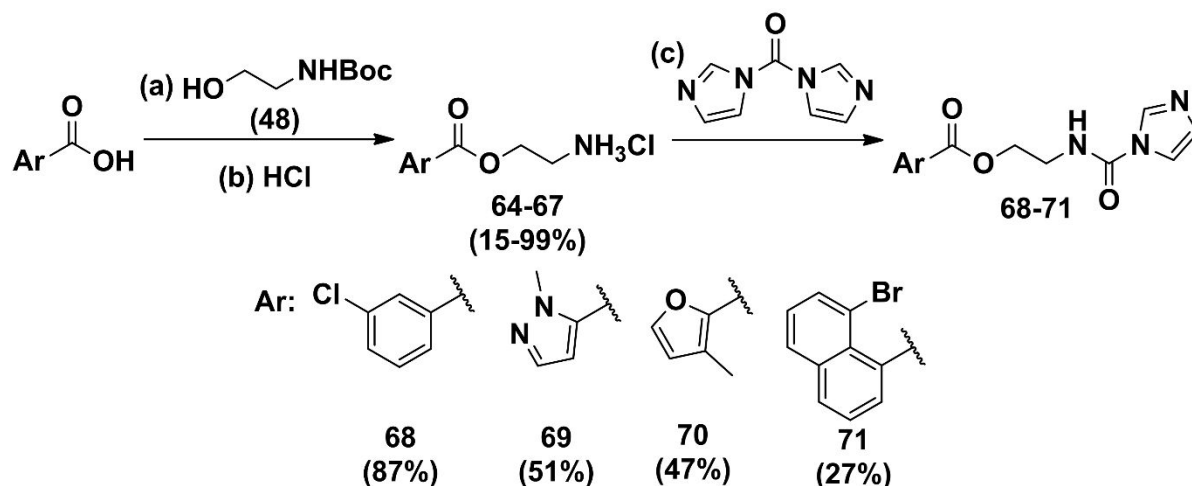
[a]Reagents and conditions: (a) **48**, EDC, DMAP, DCM, rt, 3-4 h; (b) HCl (4M in dioxane), DCM, rt, 3-5 h; (c) CDI, DMF, rt, 5-6 h.

To probe the relevance of the imidazole group present in virtual screening hit **1** for activity toward cruzain, structurally related heterocyclic derivatives were prepared (Scheme 6). Treatment of anilines **72** and **73** with bromoacetyl bromide under Schotten–Baumann conditions followed by displacement of the bromide with sodium azide afforded azides **74** and **75**. Reduction of the azide group using Pd/C and H_2, followed by coupling with 5-pyrimidinecarboxylic acid, nicotinic acid, and 1*H*-imidazole-5-carboxylic acid led to amides **76-79**. Pyrimidine, pyridine, and imidazole derivatives **80-82** were prepared from ammonium hydrochloride salt **15** by amidation with the corresponding carboxylic acid (Scheme 6). Amide **84** was prepared from an

21

S$_N$2 reaction between *m*-cresol and ethyl 2-bromoacetate followed by basic hydrolysis of the ethyl ester and acylation with CDI. Ureas **85-92** were prepared from **1** by a carbonyl substitution reaction using different amines (Scheme 7). See the Supporting Information for additional data on the synthesis of the compounds.

Scheme 6. Synthesis of heterocyclic derivatives 76-82[a]
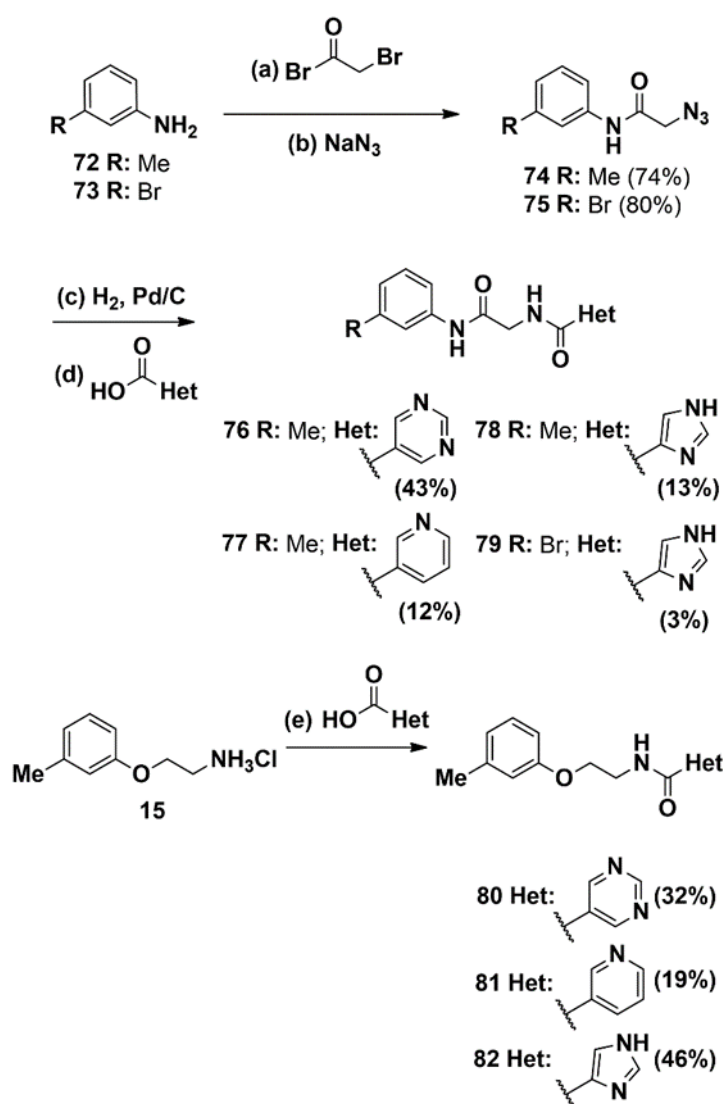
[a]Reagents and conditions: (a) bromoacetyl bromide, EtOAc, NaHCO$_3$, 0 °C to rt, 1-3 h; (b) sodium azide, DMF, rt, 18-48 h; (c) H$_2$, 5% Pd/C, MeOH, rt, 1-2 h; (d)

1
2
3
4
5
6
7
8
9
10
11
12
13
14
15
16
17
18
19
20
21
22
23
24
25
26
27
28
29
30
31
32
33
34
35
36
37
38
39
40
41
42
43
44
45
46
47
48
49
50
51
52
53
54
55
56
57
58
59
60

carboxylic acid, EDC, DMF, rt, 18 h; (e) carboxylic acid, EDC, HOBt, Et₃N, DMF, rt,

15-18 h.

Scheme 7. Synthesis of amide 84 and ureas 85-92[a]
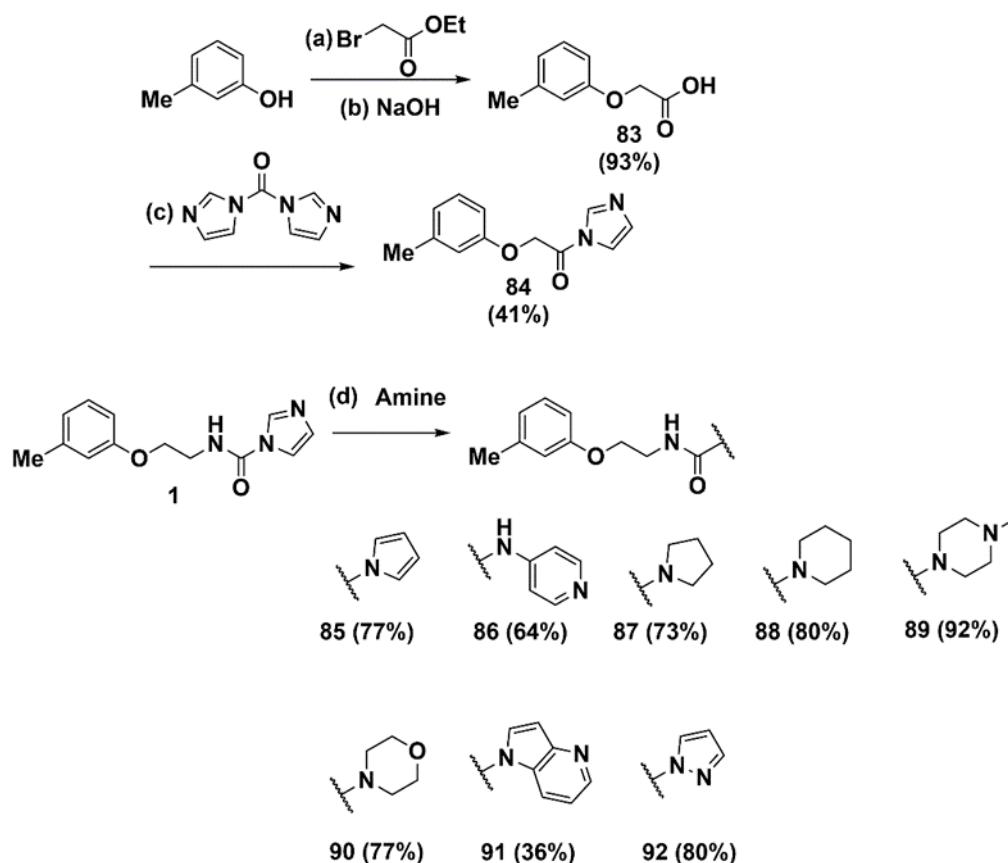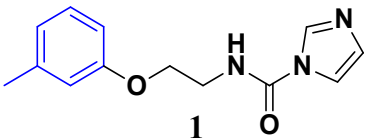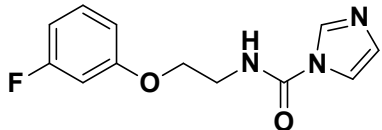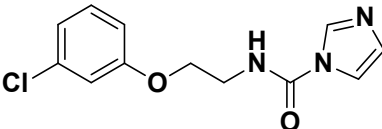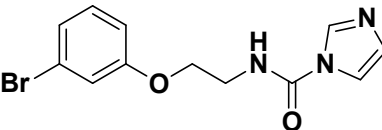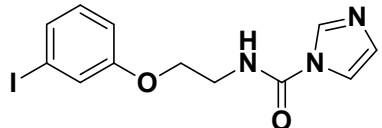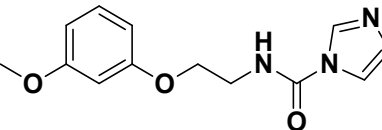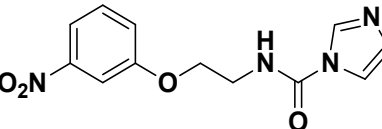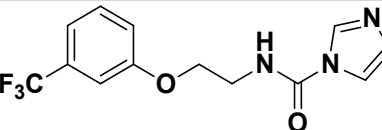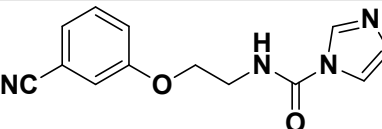
[a]Reagents and conditions: (a) ethyl 2-bromoacetate, K_2CO_3, DMF, rt, 3 h; (b) I) NaOH

(6M), MeOH, rt, 10 min; II) HCl (6M), 0°C, 10 min; (c) CDI, CH₃CN, rt, 8 h; (d)

Amine, NaH for 85 and 86, DMF, rt or 100°C, 6-14 h.

Structure-Activity Relationships and the Discovery of Cruzain Inhibitors with *in vitro* Trypanocidal Activity

Modification of the phenyl ring of inhibitor **1** was explored by adding diverse substituents to it and by expanding it to a naphthyl, leading to compounds **28-39**, **45**, **46** and **50**. Some of these analogs showed increased potency toward cruzain (1.5- to 8.3-fold) compared to **1** (Table 1). Otherwise, inhibitors **28**, **32**, **35-37, 39** and **50** proved to be less active, with the potency loss ranging from 1.7- to 3.1-fold.

The data in Table 1 indicate that modifying the phenyl ring, which interacts with the S2 subsite in the cruzain binding cavity, is a worthwhile strategy to increase the potency against the enzyme. Replacing the *m*-methyl group on the phenyl ring with a chlorine or bromine improved potency as observed for compounds **29** and **30** (IC_{50} = 0.57 and 0.41 µM, respectively). Compound **31** (IC_{50} = 0.36 µM), which has an iodine replacing the methyl, was approximately 3-fold more potent than **1**. Among compounds having a halogen at the *meta* position, *m*-fluorophenyl derivative **28** exhibited a moderate decrease in potency, showing an IC_{50} value of 1.7 µM.

24

Table 1. Structure and cruzain inhibitory activity of analogs **28-39, 45, 46** and **50** having phenyl group modifications (compound **1** as reference).

Compound	Structure	% Inhibition[a]	IC$_{50}$ (μM)[b]
28		100	1.7 ± 0.2
29		100	0.57 ± 0.03
30		100	0.41 ± 0.02
31		100	0.36 ± 0.07
32		100	2.5 ± 0.5
33		100	0.5 ± 0.1
34		100	0.50 ± 0.08
35		100	1.80 ± 0.01

25

36		100	2.8 ± 0.6
37		100	3.1 ± 0.9
38		100	0.60 ± 0.06
39		100	1.8 ± 0.3
45		100	0.12 ± 0.02
46		100	0.66 ± 0.01
50		100	3.0 ± 0.2
93[c]		100	0.21 ± 0.01

[a]The percent inhibition values are the average of three measurements (inhibitor concentration = 100 μM). [b]The IC_{50} values were determined by obtaining rate measurements in triplicate for at least six inhibitor concentrations. [c]Positive control. The values represent the mean of three individual experiments.

These results revealed that the greater the atomic radius of the halogen substituent at the *meta* position, the higher the activity. This correlation indicates that bulkier groups at this position promote a better interaction between the phenyl ring and the S2 subsite, as observed in the molecular modeling studies. Adding a bromine at the *ortho* or *para* position resulted in a potency loss of approximately 3-fold, as observed for compounds **36** and **37** (IC_{50} = 2.8 and 3.1 µM, respectively). Likewise, introducing a *meta-* and *para*-fluorine led to a moderate potency loss, as noted for inhibitor **39** (IC_{50} = 1.8 µM). Similarly, attaching a nitrile group led to a moderate potency reduction (**35**, IC_{50} = 1.80 µM), and adding a methoxy decreased activity by 2.5-fold (**32**, IC_{50} = 2.5 µM). Otherwise, adding electron-withdrawing groups such as a nitro group at the *meta* position (**33**, IC_{50} = 0.5 µM) and trifluoromethyl at the *meta* (**34**, IC_{50} = 0.5 µM) and *para* (**38**, IC_{50} = 0.6 µM) positions led to more potent inhibitors. Replacing the phenyl with a 2-bromopyridyl, a less hydrophobic fragment (**50**, IC_{50} = 3.0 µM) led to a 3-fold less active ligand.

In general, introducing bulkier substituents at the phenyl moiety resulted in more potent inhibitors. Naphthyl derivative **46**, yielding an IC_{50} value of 0.66 µM, was nearly 1.5-fold more potent than **1**. The best compound in this initial series, bromonaphthyl **45** (IC_{50} = 0.12 µM), showed an activity increment of approximately 8-fold over **1**. As shown in the molecular docking studies, the bromonaphthyl occupies the same binding site region as the *m*-tolyl of **1** (Figure 3); this phenomenon reinforces the argument that bulkier groups capable of interacting more extensively with the S2 subsite are able to improve the activity of cruzain inhibitors. These

27

findings are consistent with the results reported in our previous publication on cruzain.[12]
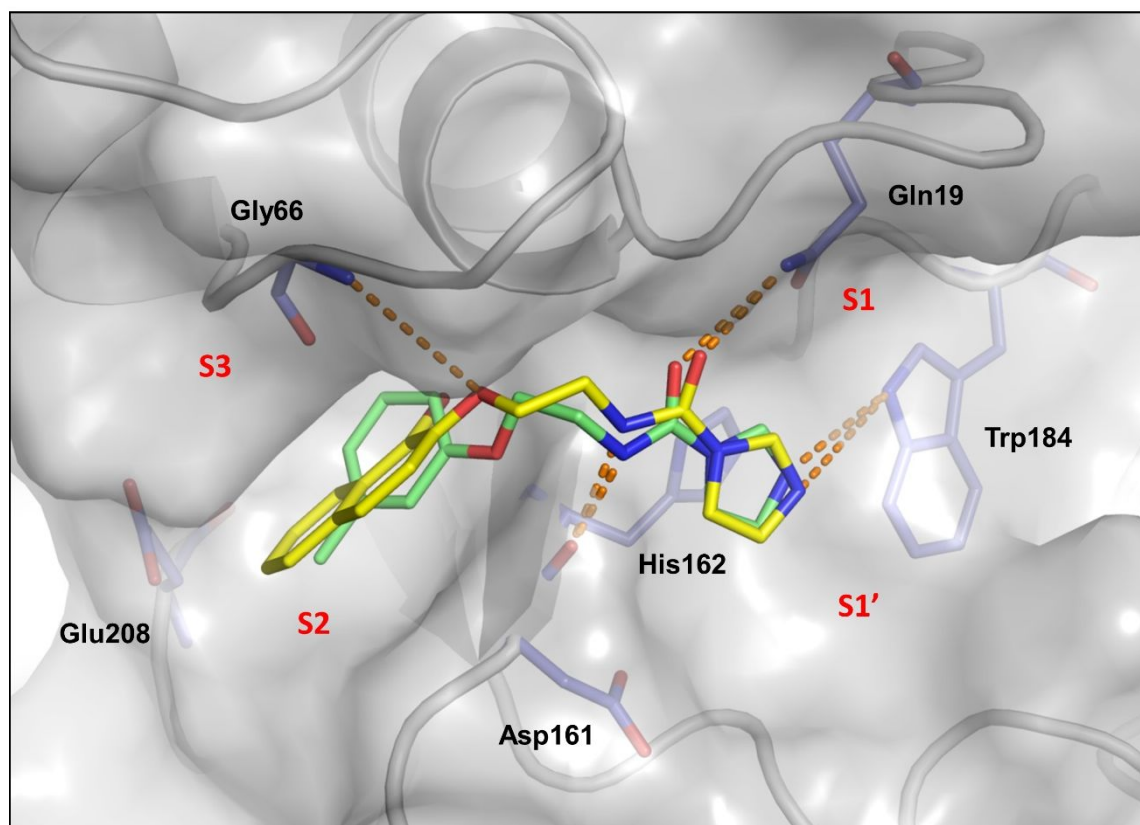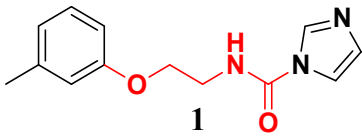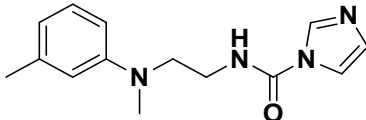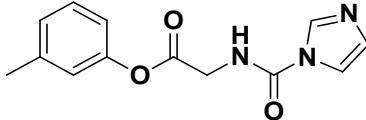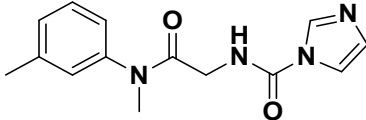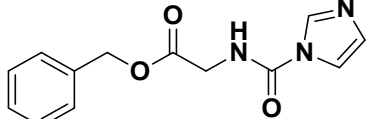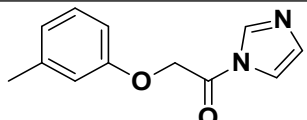

Figure 3. Binding modes of inhibitors 1 and 45. Cruzain is depicted in cartoon and surface representations (PDB 3KKU, 1.28 Å). Cruzain amino acid residues (carbon in blue) and inhibitors **1** (carbon in green) and **45** (carbon in yellow) are illustrated as sticks. Subsites in the cruzain binding site are labeled S1, S1', S2 and S3. Intermolecular interactions are indicated as dashed lines.

Further molecular modifications focused on the linker between the phenyl and imidazole rings (Table 2). Thus, seven compounds were synthesized bearing modifications to this fragment, particularly by introducing amine, amide, ester, methyl and piperazine groups. Tertiary amine **56** showed a potency increase of approximately

28

2-fold (IC_{50} = 0.52 µM) over compound **1**. Inhibitor **60** (IC_{50} = 2.0 µM), having an ester group on the linker, showed a 2-fold potency decrease. Amide **61** displayed a more pronounced activity decline, having an IC_{50} value of 6.2 µM. Compound **84** proved to be inactive, which can be related to the shortening of the linker and the resulting loss of the key interactions, such as the hydrogen bond from the urea fragment of **1**, supporting the activity of the inhibitors. The benzyl derivative **63** (IC_{50} = 0.6 µM), having a methylene and a carbonyl added to the linker and the methyl removed from the phenyl, showed an improved inhibition profile over **1**. This enhanced activity could be related to the introduction of the methylene, which projected the phenyl group more deeply into the S2 subsite, compensating for the loss of the *m*-methyl. The introduction of a rotatable bond by adding a methylene in the linker of **63**, which consequently placed the phenyl deeper into S2, reinforced the rationale that optimizing the steric complementarity with S2 is favorable for activity. In addition, the added carbonyl was observed to act as a hydrogen bond acceptor for the main chain nitrogen of Gly66, enhancing the interaction with the S3 subsite (Figure 4).

Table 2. Structure and activity against cruzain for analogs **56**, **60**, **61**, **63**, and **84** having modifications on the linker fragment (compound **1** as reference).

1

Compound	Structure	% Inhibition[a]	IC$_{50}$ (μM)[b]
56		100	0.525 ± 0.005
60		100	2.0 ± 0.1
61		100	6.2 ± 0.9
63		100	0.6 ± 0.1
84		9	ND

[a]The percent inhibition values are the average of three measurements (inhibitor concentration = 100 μM). [b]The IC$_{50}$ values were determined by obtaining rate measurements in triplicate for at least six inhibitor concentrations. The values represent the mean of three individual experiments. ND = not determined.
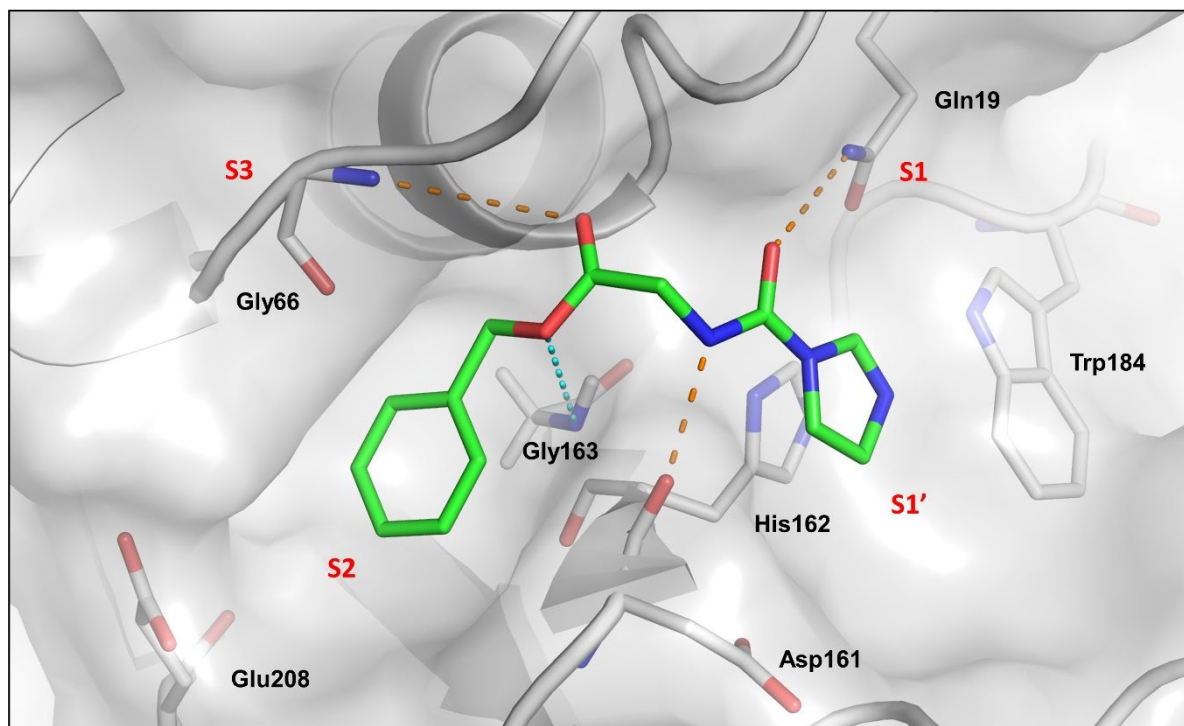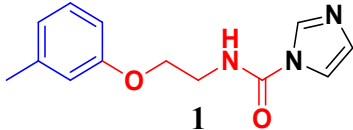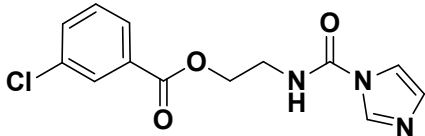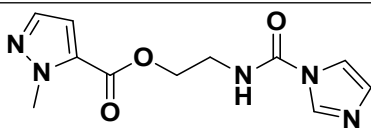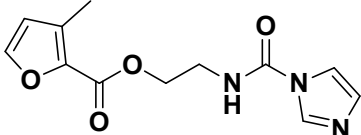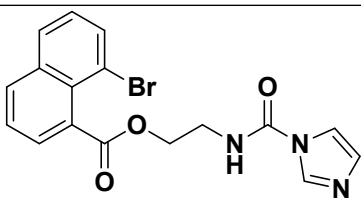
Figure 4. Binding mode of inhibitor **63**. Cruzain is depicted in cartoon and surface representations. Cruzain amino acid residues (carbon in white) and inhibitor **63** (carbon in green) are illustrated as sticks. Subsites in the cruzain binding site are labeled S1, S1', S2 and S3. Intermolecular interactions are indicated as dashed lines

The molecular optimization campaign also involved simultaneous modifications on both the phenyl ring and the linker. New analogs were synthesized with an ester carbonyl linked to several aromatic systems, such as *m*-chlorophenyl, 1-methylpyrazole, 3-methylfuran, and 8-bromo-1-naphthyl (**68-71**, respectively, Table 3). Chlorophenyl derivative **68** (IC_{50} = 0.70 μM) was moderately more potent than **1**, probably because of the additional bulk provided by the *m*-chloro, which could improve the interaction with the S2 subsite. However, replacing the phenyl with 1-methylpyrazole and 3-methylfuran caused a significant drop in the activity, as noted

31

for compounds **69** (IC$_{50}$ = 4.8 µM) and **70** (IC$_{50}$ = 3.23 µM), respectively. Compound

71 (IC$_{50}$ = 0.75 µM), having an 8-bromo-1-naphthyl core, displayed a discrete activity

improvement compared to **1** but was less potent than the 1-bromo-2-naphthyl

derivative **45**. Adding the extra carbonyl to provide an extension of the linker was

effective only when combined with an expansion of the phenyl, which is the case for

inhibitors **68** and **71**.

Table 3. Structure and activity on cruzain for analogs **68-71** having modifications on

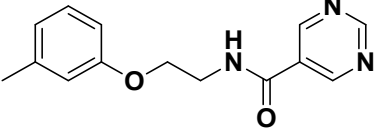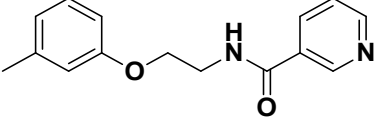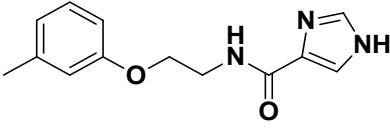both the linker and the phenyl (compound **1** as reference).

1
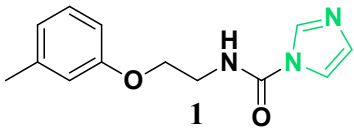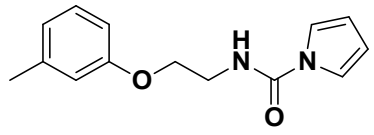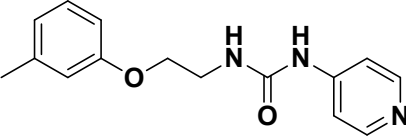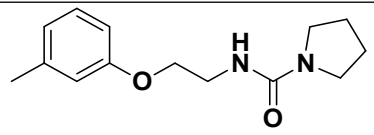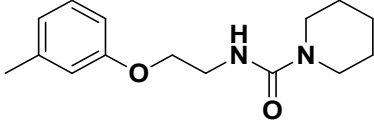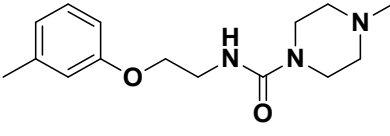
Compound	Structure	% Inhibition[a]	IC$_{50}$ (µM)[b]
68		100	0.70 ± 0.07
69		100	4.8 ± 0.3
70		100	3.23 ± 0.66
71		100	0.75 ± 0.04

[a]The percent inhibition values are the average of three measurements (inhibitor

concentration = 100 µM). [b]The IC$_{50}$ values were determined by obtaining rate

measurements in triplicate for at least six inhibitor concentrations. The values represent the mean of three individual experiments.
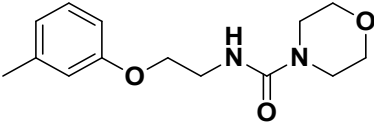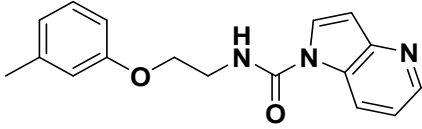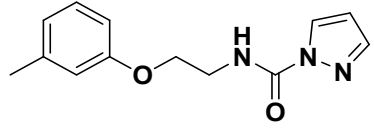
To probe the relevance of the imidazole moiety on the activity of the cruzain inhibitors, a series of acyl heterocycles (aromatic and nonaromatic) was prepared (compounds **80-82** and **85-92**, Table 4). The 1-substituted imidazole ring and urea functional groups were shown to be important for cruzain inhibition; compounds lacking these groups proved inactive. Inactivity was observed when exchanging the imidazole with other *N*-aromatic groups and linking them to the carbonyl via carbon-carbon bonding (amide functional group) as in compounds **80-82**, as well as exchanging the imidazole group with an aminopyridine (**86**) and other nonaromatic heterocycles (**87-90**). Of this series, pyrrole, azaindole and pyrazole derivatives **85**, **91** and **92**, respectively, displayed inhibition above 50% at 100 μM. Pyrrole **85** showed low potency (IC$_{50}$ = 77 μM); however, **91** and **92**, having more than one nitrogen in the heteroaromatic ring, showed IC$_{50}$ values of 3.2 and 6.2 μM, respectively. As illustrated in Figures **2** and **3,** the 1-substituted imidazole in the inhibitor interacts with the S1' subsite by forming a hydrogen bond with the side chain indole nitrogen of Trp184, and the carbonyl of the inhibitor urea fragment interacts with the S1 subsite by hydrogen bonding with Gln19. These results suggest that the activity of **91** and **92** is likely due to the structural similarities between the pyrazole and azaindole fragments with imidazole, generating the same electronic effect on the carbonyl and presenting a nitrogen in the aromatic ring to make a hydrogen bonding interaction with Trp184.

33

Table 4. Structure and activity on cruzain for analogs **80-82** and **85-92** with modifications to the imidazole (compound **1** as reference).

1

Compound	Structure	% Inhibition[a]	IC$_{50}$ (µM)[b]
80		4	ND
81		8	ND
82		2	ND
85		51	77 ± 8
86		3	ND
87		-	ND
88		17	ND
89		7	ND

90		9	ND
91		93	3.2 ± 0.1
92		78	6.2 ± 0.3

[a]The percent inhibition values are the average of three measurements (inhibitor concentration = 100 μM). [b]The IC_{50} values were determined by obtaining rate measurements in triplicate for at least six inhibitor concentrations. The values represent the mean of three individual experiments. ND = not determined.

The SBDD approach outlined in this study was aimed at identifying competitive cruzain inhibitors. Given the competitive inhibition mechanism of **1** (Figure 1), the designed analogs would be expected to have the same mode of action. Therefore, additional enzyme kinetics studies were carried out to determine the mechanism of inhibition of the most potent molecules. The competitive mechanism was confirmed for inhibitors **31**, **45**, **63** and **71**, as shown in the Lineweaver−Burk plots in Figure 5. The maximum velocity values ($1/V_{max}$), which are the intersections with the y-axis, did not change with increasing inhibitor concentration (I), as expected for competitive inhibitors. Typical of a competitive mode of inhibition, the apparent Michaelis–Menten constant ($K_M^{app} = -1/K_M$), which is given by the intersection with the x-axis, increased with growing I. The dissociation constants for the enzyme-inhibitor complexes (K_i values) were determined by taking the values of K_M^{app} for the

different I values. These results confirmed that the designed analogs of **1** interact with the cruzain active site, inhibiting its catalytic activity by a competitive mechanism.
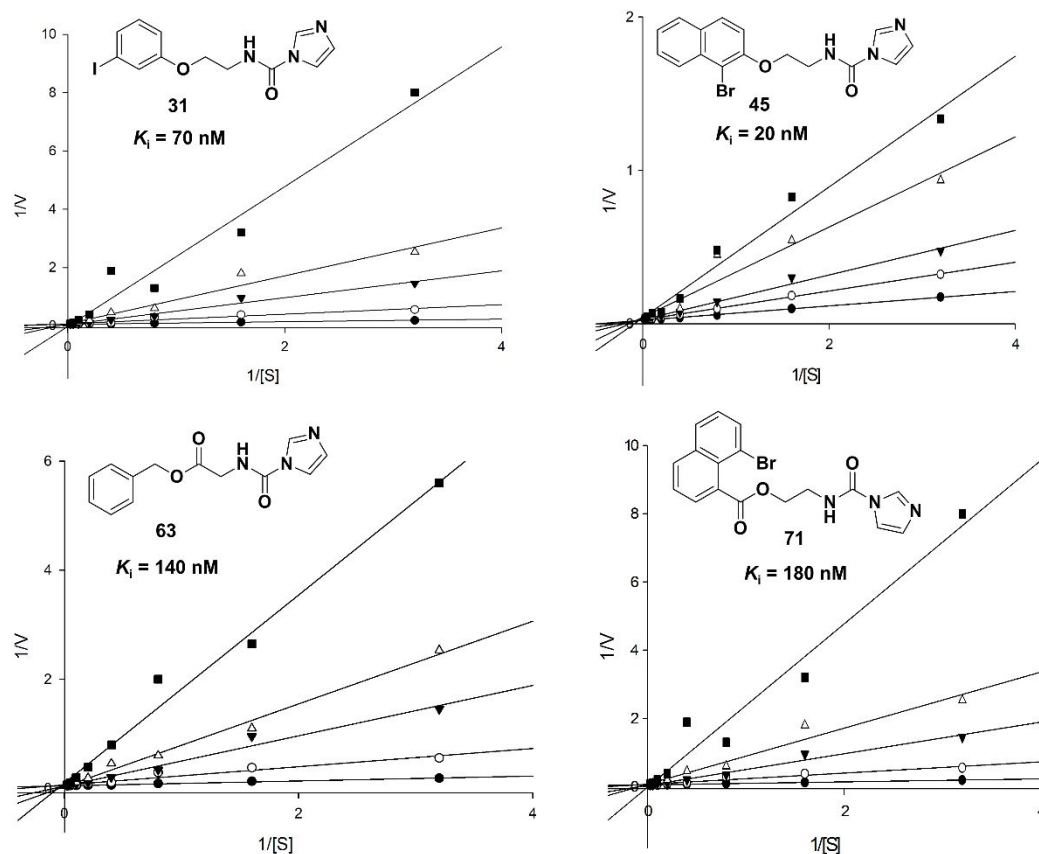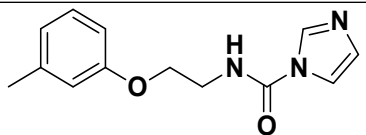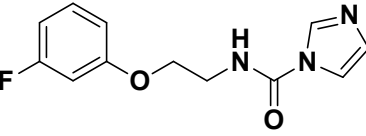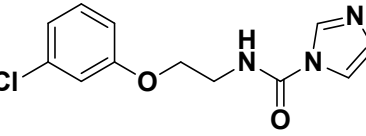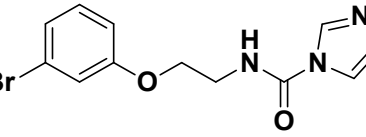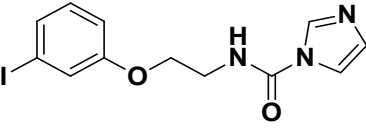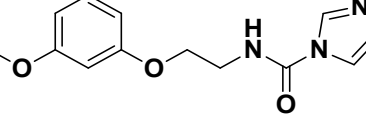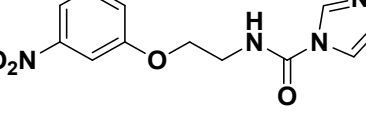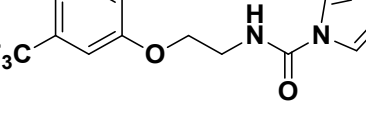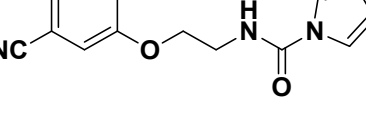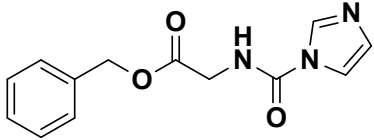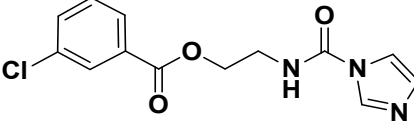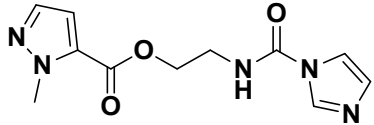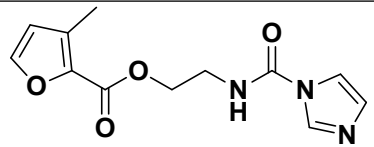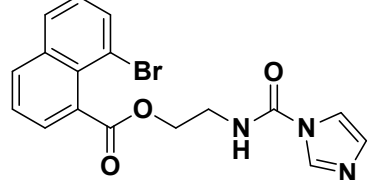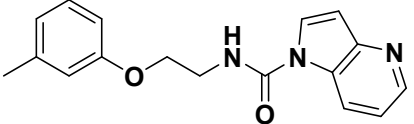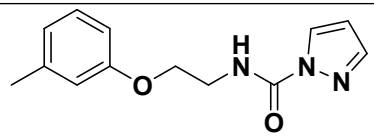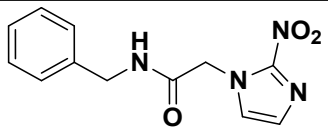

Figure 5. Lineweaver-Burk plots for cruzain inhibitors **31**, **45**, **63** and **71**. Curves refer to the following inhibitor concentrations: control – no inhibitor (●); 0.2 µM (○); 0.4 µM (▼); 0.8 µM (△) and 1.6 µM (■).

Given the results of the 36 cruzain inhibitors, the next step was to evaluate their activity against intracellular *T. cruzi* amastigotes (Table 5). A subset of 26 compounds was tested along with the reference drug **BZ**. Cell viability assays using human HFF-1 fibroblasts were conducted in parallel to evaluate compound cytotoxicity and selectivity.

36

Table 5. Trypanocidal and cytotoxic activity of the most potent cruzain inhibitors against intracellular *T. cruzi* amastigotes and HFF-1 human fibroblasts.

Compound	Structure	IC$_{50}$ (µM) *T. cruzi*[a]	IC$_{50}$ (µM) HFF-1[b]	SI[c]
1		1.1 ± 0.3	> 100	> 86
28		31 ± 3	> 100	> 3
29		2.3 ± 0.8	> 100	> 42
30		29 ± 1	> 100	> 3
31		17 ± 4	> 100	> 5.8
32		> 100	> 100	ND
33		44 ± 4	> 100	> 2
34		3.4 ± 0.4	> 100	> 29
35		39 ± 4	>100	> 2

37

36		2.9 ± 0.4	> 100	> 33
37		2.0 ± 0.3	> 100	> 50
38		26.5 ± 0.5	> 100	> 3
39		> 100	> 100	ND
45		7.5 ± 1.2	> 50	> 6
46		26 ± 1	> 100	> 3
50		17.7 ± 0.7	> 100	> 5
56		> 100	>100	ND
60		1.7 ± 0.5	> 100	> 58
61		6 ± 1	> 30	> 4

63		13 ± 3	> 100	> 7.7
68		9 ± 1	>100	> 10
69		15 ± 2	>100	> 6
70		22 ± 3	>100	> 4
71		20 ± 3	>100	> 5
91		13 ± 5	>100	> 7
92		29 ± 6	>100	> 3
BZ		3.3 ± 0.6	>100	> 30

[a]Viability assay using intracellular *T. cruzi* amastigotes. The values are the average of three independent experiments. [b]Cytotoxicity assay. The values represent the average of two independent experiments. [c]Selectivity index ($IC_{50}^{HFF\text{-}1}/IC_{50}^{T.\ cruzi}$). ND = not determined.

Several compounds showed trypanocidal activity similar or superior to that of

BZ (IC_{50} = 3.3 µM). Compounds **1** (IC_{50} = 1.1 µM) and **60** (IC_{50} = 1.7 µM) were

approximately 3-fold more potent than the reference drug. Compounds **29** (IC_{50} = 2.3

µM), **34** (IC_{50} = 3.4 µM), **36** (IC_{50} = 2.9 µM) and **37** (IC_{50} = 2.0 µM) had anti-*T. cruzi*

activity similar to that of **BZ**. Analogs **45** (IC_{50} = 7.5 µM) and **61** (IC_{50} = 6 µM) also

displayed promising activity against the parasite.

Some points can be raised from the activity data against *T. cruzi*. Increased

steric bulk at the phenyl ring, although showing improved potency toward cruzain, did

not correlate with an enhancement in trypanocidal activity. In contrast to the pattern

observed for cruzain (*meta* being the most favorable position), the *o*-bromophenyl and

p-bromophenyl derivatives yielded the best results in the phenotypic assay. Other

potent cruzain inhibitors, such as *m*-fluorophenyl derivative **28** and 3,4-difluorophenyl

derivative **39**, were inactive against the parasite. *m*-Tolyl compounds having either an

ether or ester oxygen adjacent to the phenyl ring were the most effective trypanocidal

compounds: **1** (IC_{50} = 1.1 µM) and **60** (IC_{50} = 1.7 µM). In short, of the identified

cruzain inhibitors, *m*-tolyl derivative **1** was the most potent trypanocidal compound.

The most potent cruzain inhibitor, 1-bromonaphthyl derivative **45**, yielded an IC_{50}

value of 7.5 µM.

The cytotoxicity of the designed cruzain inhibitors was probed using HFF-1

human fibroblasts (Table 5). All synthesized compounds produced no significant toxic

effects on these cells. The ratio between the IC_{50} values for HFF-1 and *T. cruzi* was

calculated to yield the selectivity index (SI). Some cruzain inhibitors showed SI

values superior to that of the reference drug **BZ** (SI > 30), particularly those having

the most promising trypanocidal activity. Among the most selective analogs with relevant trypanocidal activity, one can highlight compounds **1** (SI > 86), **29** (SI > 42), **36** (SI > 33), **37** (SI > 50) and **60** (SI > 58); all of which featured a carboxamide-imidazole moiety.

Carbamoyl Imidazoles 1 and 45 Display No Acute Toxicity and Reduce Parasite Burden *in vivo*

Compounds **1** and **45** were finally selected for *in vivo* assays given their appropriate activity and cytotoxicity profiles. First, we determined the maximum tolerated dose of these compounds by administering increasing doses in mice and evaluating the dose at which toxic effects could be observed.[38] Each compound was intraperitoneally (i.p.) administered in female Swiss mice at single doses of 75, 100, 150 and 300 mg/kg of body weight. Parameters related to behavioral, autonomic functions, and neurological activity, along with weight and mortality, were assessed as toxicity signs. Mortality and clinical signs associated with toxicity were observed and recorded at 0.5, 2, 4, 8 and 24 hours after the single-dose administration. Next, these toxicity signs were assessed once a day for two consecutive weeks. Piloerection was observed within the first 24 hours at the highest doses (150 and 300 mg/kg, Table S1). For both compounds, animals treated at the dose of 300 mg/kg showed piloerection until day 5 after injection. Mice that received a 150 mg/kg dose had piloerection until day 2 and day 3 for compounds **1** and **45**, respectively. No mortality was observed for any dose tested. These findings indicated a low level of acute toxicity at the tested

41

doses for both cruzain inhibitors (see Table S1 in the Supporting Information for the detailed MTD results).

Considering the favorable acute toxicity results, the *in vivo* trypanocidal activity of compounds **1** and **45** was determined. Female Swiss mice were infected with *T. cruzi* (*Y* strain)[39] and treated via i.p. with seven daily doses of **BZ**, compound **1** or compound **45** (100 mg/kg of body weight). Treatment started on day 5 after infection. The following parameters were evaluated in these experiments: (i) level of parasitemia after treatment; (ii) suppression of peak parasitemia; and (iii) survival rate of animals. Parasitemia was expressed as the number of *T. cruzi* trypomastigotes per 5 µL of blood and was calculated using the Brener method.[33]

Statistical analyses using repeated measures ANOVA, considering the treatment factors and day (repeated measure)[40], showed a significant interaction between days and treatment factors ($F_{3,16}$ = 5.6, p-value < 0.05). A post hoc test indicated that the groups treated with **BZ** and the synthesized cruzain inhibitors showed a significant reduction in parasitemia compared with the group treated with vehicle (p-value < 0.05). Moreover, this analysis revealed no significant difference in the levels of parasitemia among the **BZ** group and those treated with compounds **1** and **45** (Figure 6A). On the fifth day of treatment, when parasitemia reached its peak, **BZ**, **1** and **45** decreased parasite burden by 100, 85 and 84%, respectively, when compared to the vehicle group ($F_{3,17}$ = 8.75, p-value < 0.05). These results indicate the suitable ability of both cruzain inhibitors to suppress peak parasitemia (Figure 6B).
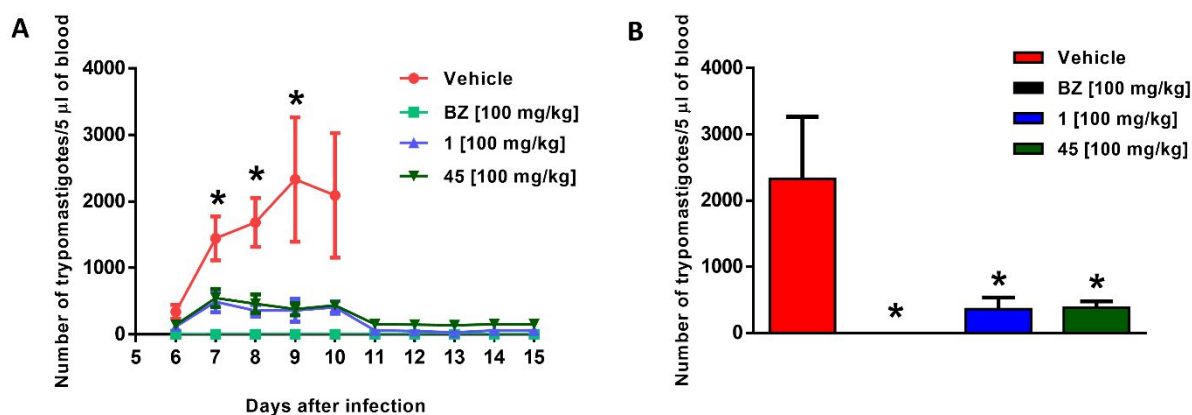
Figure 6. Reduction of parasite burden *in vivo* after treatment with compounds **1** and **45**. (A) Parasitemia during *T. cruzi* (*Y* strain) infection in mice treated with vehicle, benznidazole (**BZ**) or cruzain inhibitors **1** and **45**, expressed as the number of trypomastigotes per 5 µL of blood. Treatment consisted of seven daily doses of 100 mg/kg of body weight, starting at day 5 after infection. The data represent the mean parasitemia ± SEM (5 animals per group). Vehicle solution: 0.9% NaCl + 10% DMSO. (*$p<0.05$ when compared to other groups). (B) Peak parasitemia expressed as the number of trypomastigotes per 5 µL of blood in mice treated with vehicle, **BZ** or cruzain inhibitors **1** and **45**. The data represent the mean parasitemia ± SEM (5 animals per group). Vehicle solution: 0.9% NaCl + 10% DMSO (*$p<0.05$ when compared to vehicle and when compared to other groups).

Regarding the survival rate of treated mice, chi-square analyses showed relevant differences between the groups (p-value < 0.05). The survival rate was observed 15 days after infection. The **BZ** group did not show any mortality during this period (Figure 7). In contrast, the group treated with vehicle showed 100% mortality on day 11 after infection. The survival rate of mice that were given compounds **1** and **45** was significantly higher than that of the vehicle group. The group treated with compound **1** presented its first death on day 11 after infection. Among animals that were given compound **45**, the first death occurred on day 10 after infection.

43

Compounds **1** and **45** were able to prolong the survival of mice throughout the period

of observation.
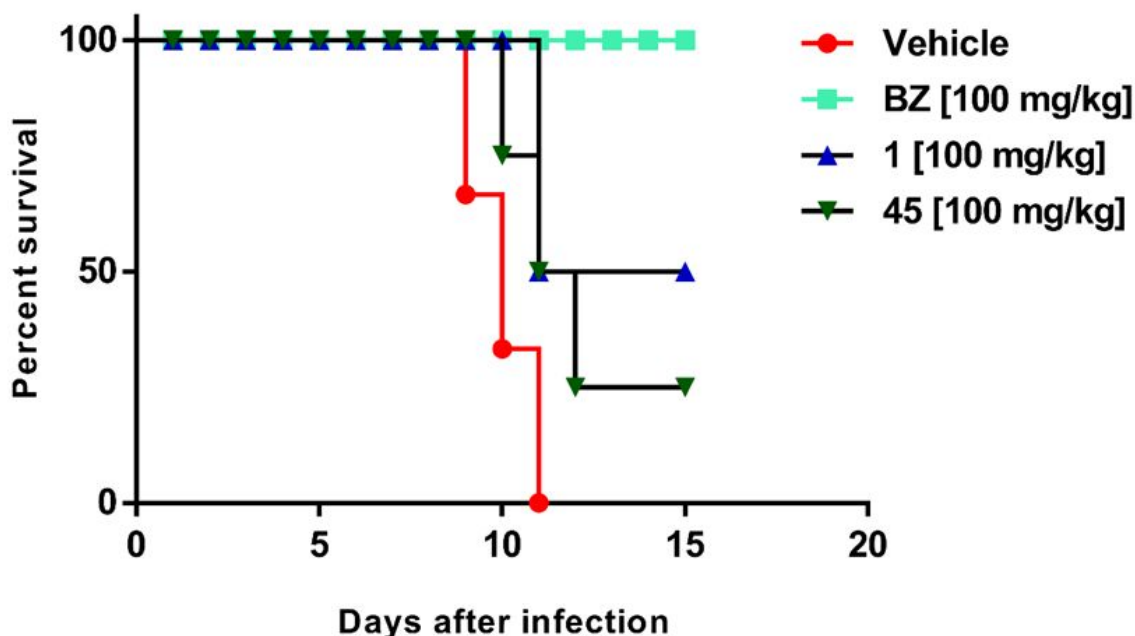
Figure 7. Survival rate of infected mouse treated with vehicle, benznidazole (BZ), or

cruzain inhibitors 1 and 45. Treatment consisted of seven daily doses of 100 mg/kg of

body weight, starting at day 5 after infection. The survival rate is expressed as the

percentage of surviving animals over the total number of mice in each group (5

animals per group). Points represent the percent survival at each day. Vehicle solution:

0.9% NaCl + 10% DMSO.

The SAR studies highlighted that the inhibitors possessing a phenyl ring

expanded with bulkier groups were active toward the enzyme. Similarly, modifying

the linker in the region next to the phenyl by adding an amine, ester, or methylene led

to potent inhibitors. Some analogs incorporating structural changes on both the phenyl

44

and the linker were also remarkably active. Molecular modeling showed that all these modifications enabled more effective interactions with the S2 and S3 pockets, consequently leading to improved inhibitors. The imidazole group proved important, and its replacement with other heterocycles led to inactive compounds, which can be associated with the loss of interactions with the S1 subsite. However, the replacement of imidazole by similar groups, such as pyrazole and azaindole, led to potent inhibitors. Following the computational and experimental data, it can be stressed that an optimal interaction with the S1 pocket is a key aspect for designing further cruzain inhibitors within this structural class.

Finally, examining the target-based and phenotypic data, one can observe a lack of clear correlation between enzyme inhibition and trypanocidal activity. For example, inhibitors **30** and **31**, although having nanomolar potency against the molecular target (IC$_{50}$ of 0.41 and 0.36 μM**,** respectively), were poorly active against *T. cruzi* (IC$_{50}$ of 29 and 17 μM, respectively). Another example, compound **56** with an IC$_{50}$ of 0.52 μM on cruzain was inactive on *T. cruzi*. This lack of a direct correlation is to some extent expected given the complexity of the cellular environment and transmembrane transport issues. Alternatively, some of the synthesized compounds, apart from being potent enzyme inhibitors, demonstrated equivalent activity in the phenotypic tests. Compound **1**, for instance, showed an IC$_{50}$ of 1 μM for cruzain alongside trypanocidal activity superior to that of the clinically used drug **BZ**. Regarding the safety profile, some compounds, such as **1**, **29**, **36**, **54** and **60**, showed a better SI than did **BZ**. The low potential of the inhibitors to produce adverse effects was additionally assessed in MTD studies. The most promising compounds, **1** and **45**,

reduced parasite burden as efficiently as **BZ** and showed minor *in vivo* toxicity and no mortality at doses as high as 300 mg/kg. These are rewarding findings given that toxicity is one of the major causes of attrition in drug R&D.

CONCLUSION

Our integrated SBDD approach involving compound libraries, virtual screening, organic synthesis, molecular modeling, protein target-based, phenotypic and *in vivo* studies led us to the discovery of potent, reversible and nonpeptidic cruzain inhibitors with significant trypanocidal activity. The enzyme kinetics data allowed for the construction of robust SAR studies, which were used to disclose some key structural features related to the activity of this series of compounds. Moreover, the insights into the enzyme-inhibitor recognition process learned during the molecular optimization efforts were consistent with the experimentally determined mechanism of inhibition. Along with a suitable toxicity profile, the most promising compounds (**1** and **45**) reduced the parasitemia levels as effectively as **BZ** did after seven days of treatment. This series of inhibitors represents an important advancement to overcome the weaknesses associated with the clinical development of covalent compounds. The knowledge of the reversible competitive mechanisms of enzyme inhibition for this class of carbamoyl imidazoles, along with all the collected *in vitro* and *in vivo* results, can be used to guide the development of these new cruzain inhibitors with trypanocidal activity. Given the long-standing lack of therapeutic innovation and the shortcomings of current chemotherapy, this novel class of cruzain

46

inhibitors can represent a new pathway to be explored in Chagas disease drug discovery.

SUPPORTING INFORMATION

Supporting figures and tables, materials and methods for synthesis and characterization of compounds and NMR spectra.

ACKNOWLEDGMENTS

REFERENCES

(1) Pérez-Molina, J.A.; Molina, I. Chagas disease. *Lancet* **2018**, *391*, 82-94.

(2) Bern, C. Chagas' Disease. *N. Engl. J. Med*. **2015**, *373*, 456-466.

(3) World Health Organization Home Page. http://www.who.int/chagas/en/ (accessed May 30, 2019).

(4) Castro, J.A.; de Mecca, M.M.; Bartel, L.C. Toxic side effects of drugs used to treat Chagas' disease (American trypanosomiasis). *Hum. Exp. Toxicol*. **2006**, *25*, 471-479.

(5) Ferreira, L.L.G.; Andricopulo, A.D. Drugs and vaccines in the 21st century for neglected diseases. *Lancet Infect. Dis.* **2019**, *19*, 125-127.

(6) Martinez-Mayorga, K.; Byler, K. G.; Ramirez-Hernandez, A. I.; Terrazas-Alvares, D. E. Cruzain inhibitors: efforts made, current leads and a structural outlook of new hits. *Drug Discov. Today* **2015**, *7*, 890-898.

(7) Ferreira, L. G.; Andricopulo, A. D. Targeting cysteine proteases in trypanosomatid disease drug discovery. *Pharmacol. Ther.* **2017**, *180*, 49-61.

(8) Doyle, P. S.; Zhou, Y. M.; Hsieh, I.; Greenbaum, D. C.; McKerrow, J. H.; Engel, J. C. The *Trypanosoma cruzi* protease cruzain mediates immune evasion. *PLoS Pathog.* **2011**, *7*, e1002139.

(9) Ndao, M.; Beaulieu, C.; Black, W. C.; Isabel, E.; Vasquez-Camargo F.; Nath-Chowdhury, M.; Massé, F.; Mellon, C.; Methot, N.; Nicoll-Griffith, D. A. Reversible cysteine protease inhibitors show promise for a Chagas disease cure. *Antimicrob. Agents Chemother.* **2014**, *2*, 1167-1178.

(10) Goupil, L.S., & McKerrow, J.H. (2014). Introduction: drug discovery and development for neglected diseases. *Chem. Rev. 114*, 11131-11137.

(11) Neitz, R. J.; Bryant, C.; Chen, S.; Gut, J.; Caselli, E. H.; Ponce, S.; Chowdhury, S.; Xu, H.; Arkin, M. R.; Ellman, J. A.; Renslo, A. R. Tetrafluorophenoxymethyl ketone cruzain inhibitors with improved pharmacokinetic properties as therapeutic leads for Chagas' disease. *Bioorg. Med. Chem. Lett*. **2015**, *21*, 4834-4837.

(12) Ferreira, R. S.; Dessoy, M. A.; Pauli, I.; Souza, M. L.; Krogh, R.; Sales, A. I.; Oliva, G.; Dias, L. C.; Andricopulo, A. D. Synthesis, biological evaluation, and

48

structure-activity relationships of potent noncovalent and nonpeptidic cruzain inhibitors as anti-Trypanosoma cruzi agents. *J. Med. Chem*. **2014**, *6*, 2380-2392.

(13) Brak, K.; Kerr, I. D.; Barrett, K. T, Fuchi, N.; Debnath, M.; Ang, K.; Engel, J. C.; McKerrow, J. H.; Doyle, P. S.; Brinen, L. S.; Ellman, J. A. Nonpeptidic tetrafluorophenoxymethyl ketone cruzain inhibitors as promising new leads for Chagas disease chemotherapy. *J. Med. Chem*. **2010**, *4*, 1763-1773.

(14) Rogers, K. E.; Keränen, H.; Durrant, J. D.; Ratnam, J.; Doak, A.; Arkin, M. R.; McCammon, J. A. Novel cruzain inhibitors for the treatment of Chagas' disease. *Chem. Biol. Drug Des*. **2012**, *3*, 398-405.

(15) Avelar, L. A.; Camilo, C. D.; de Albuquerque, S.; Fernandes, W. B.; Gonçalez, C.; Kenny, P. W.; Leitão, A.; McKerrow, J. H.; Montanari, C. A.; Orozco, E. V.; Ribeiro, J. F.; Rocha, J. R.; Rosini, F.; Saidel, M. E. Molecular Design, Synthesis and Trypanocidal Activity of Dipeptidyl Nitriles as Cruzain Inhibitors. *PLoS Negl. Trop. Dis*. **2015**, *7*, e0003916.

(16) Espíndola, J. W.; Cardoso, M. V.; Filho, G. B.; Oliveira, E.; Silva, D. A.; Moreira, D. R.; Bastos, T. M.; Simone, C. A.; Soares, M. B.; Villela, F. S.; Ferreira, R. S.; Castro, M. C.; Pereira, V. R.; Murta, S. M.; Sales Junior, P. A.; Romanha, A. J.; Leite, A. C. Synthesis and structure-activity relationship study of a new series of antiparasitic aryloxyl thiosemicarbazones inhibiting Trypanosoma cruzi cruzain. *Eur. J. Med. Chem*. **2015**, *101*, 818-835.

(17) Doyle, P. S.; Zhou, Y. M.; Engel, J. C.; McKerrow, J. H. A cysteine protease inhibitor cures Chagas' disease in an immunodeficient-mouse model of infection. *Antimicrob. Agents Chemother*. **2007**, *51*, 3932–3939.

(18) Kerr, I. D.; Lee, J. H.; Farady, C. J.; Marion, R.; Rickert, M.; Sajid, M.; Pandey, K. C.; Caffrey, C. R.; Legac, J.; Hansell, E.; McKerrow, J. H.; Craik, C. S.; Rosenthal, P. J.; Brinen, L. S. Vinyl sulfones as antiparasitic agents and a structural basis for drug design. *J. Biol. Chem*. **2009**, *284*, 25697-25703.

(19) Irwin, J. J.; Sterling, T.; Mysinger, M. M.; Bolstad, E. S.; Coleman, R. G. ZINC: a free tool to discover chemistry for biology. *J. Chem. Inf. Model*. **2012**, *7*, 1757-1768.

(20) Ferreira, R.S.; Simeonov, A., Jadhav, A.; Eidam, O., Mott, B.T.; Keiser, M.J.; McKerrow, J.H.; Maloney, D.J.; Irwin, J.J.; Shoichet, B.K. Complementarity between a docking and a high-throughput screen in discovering new cruzain inhibitors. *J. Med. Chem*. **2010**, *53*, 4891-4905.

(21) Shoichet, B. K.; Leach, A. R.; Kuntz, I. D. Ligand solvation in molecular docking. *Proteins* **1999**, *1*, 4-16.

(22) Meng, E. C.; Shoichet, B. K.; Kuntz, I. D. Automated docking with grid-based energy evaluation. *J. Comput. Chem*. **1992**, *4*, 505-524.

(23) Gilson, M. K.; Honig, B. H. Calculation of electrostatic potentials in an enzyme active site. *Nature* **1987**, *6143*, 84-86.

(24) Verdonk, M. L.; Cole, J. C.; Hartshorn, M. J.; Murray, C. W.; Taylor, R. D. Improved protein-ligand docking using GOLD. *Proteins*, **2003**, *4*, 609-623.

(25) Jain, A. N. Surflex: fully automatic flexible molecular docking using a molecular similarity-based search engine. *J. Med. Chem*. **2003**, *4*, 499-511.

(26) Jain, A. N. Surflex-Dock 2.1: robust performance from ligand energetic modeling, ring flexibility, and knowledge-based search. *J. Comput. Aided Mol. Des*. **2007**, *5*, 281-306.

(27) Lill, M. A.; Danielson, M. L. Computer-aided drug design platform using PyMOL. J. *Comput. Aided Mol. Des*. **2011**, *1*, 13-19.

(28) Pettersen, E. F.; Goddard, T. D.; Huang, C. C.; Couch, G. S.; Greenblatt, D. M.; Meng, E. C.; Ferrin, T. E. UCSF Chimera--a visualization system for exploratory research and analysis. *J. Comput. Chem.* **2004**, *13*, 1605-1612.

(29) Buckner, F. S.; Verlinde, C.L.; La Flamme, A. C.; Van Voorhis, W. C. Efficient technique for screening drugs for activity against Trypanosoma cruzi using parasites expressing beta-galactosidase. *Antimicrob. Agents Chemother*. **1996**, *11*, 2592-2597.

(30) Goodwin, C. J.; Holt, S. J.; Downes, S.; Marshall, N. J. Microculture tetrazolium assays: a comparison between two new tetrazolium salts, XTT and MTS. *J. Immunol. Methods* **1995**, *1*, 95-103.

(31) Lorke, D. A new approach to practical acute toxicity testing. *Arch. Toxicol.* **1983**, *4*, 275-287.

(32) Filardi, L. S.; Brener, Z. Susceptibility and natural resistance of Trypanosoma cruzi strains to drugs used clinically in Chagas disease. *Trans. R. Soc. Trop. Med. Hyg*. **1987**, *5*, 755-759.

(33) Brener, Z. Therapeutic activity and criterion of cure on mice experimentally infected with Trypanosoma cruzi. *Rev. Inst. Med. Trop. Sao Paulo* **1962**, *4*, 389-396.

(34) O'Brien, T. C.; Mackey, Z. B.; Fetter, R. D.; Choe, Y.; O'Donoghue, A. J.; Zhou, M.; Craik, C. S.; Caffrey, C. R.; McKerrow, J. H. A parasite cysteine protease is key to host protein degradation and iron acquisition. *J. Biol. Chem*. **2008**, *43*, 28934-28943.

51

(35) Feng, B. Y.; Shoichet, B. K. A detergent-based assay for the detection of promiscuous inhibitors. *Nat. Protoc*. **2006**, *2*, 550-553.

(36) Hopkins, A. L.; Keserü, G. M..; Leeson, P. D.; Rees, D. C.; Reynolds, C. H. The role of ligand efficiency metrics in drug discovery. *Nat. Rev. Drug Discov*. **2014**, *2*, 105-121.

(37) Bembenek, S. D.; Tounge, B. A.; Reynolds, C. H. Ligand efficiency and fragment-based drug discovery. *Drug Discov. Today* **2009**, *5-6*, 278-283.

(38) Roberts, R. A.; Kavanagh, S. L.; Mellor, H. R.; Pollard, C. E.; Robinson, S.; Platz, S. J. Reducing attrition in drug development: smart loading preclinical safety assessment. *Drug Discov. Today* **2014**, *3*, 341-347.

(39) Rodriguez, H. O.; Guerrero, N. A.; Fortes, A.; Santi-Rocca, J.; Gironès, N.; Fresno, M. Trypanosoma cruzi strains cause different myocarditis patterns in infected mice. *Acta Trop*. **2014**, *139*, 57-66.

(40) Statistics Solutions Home Page. http://www.statisticssolutions.com/manova-analysis-anova/ (accessed May 23, 2019).

1
2
3
4
5
6
7
8
9
10
11
12
13
14
15
16
17
18
19
20
21
22
23
24
25
26
27
28
29
30
31
32
33
34
35
36
37
38
39
40
41
42
43
44
45
46
47
48
49
50
51
52
53
54
55
56
57
58
59
60

Table of Contents Graphic

$IC_{50}^{cruzain} = 1.0\ \mu M$

$K_i = 120\ nM$

$IC_{50}^{T.\ cruzi} = 1.1\ \mu M$